Supporting Information

Covalent Bonding Modulated Graphene-Metal Interfacial Thermal Transport

Tao Jiang[A†], Xueqiang Zhang[B,C†], Suresh Vishwanath[D,E†], Xin Mu[A†], Vasily Kanzyuba[D], Denis A. Sokolov[B], Sylwia Ptasinska [B,F], David B. Go[A,G], Huili Grace Xing[D,E,H], Tengfei Luo[A,I]*

[A] Department of Aerospace and Mechanical Engineering, University of Notre Dame, Notre Dame, IN 46556, USA

[B] Radiation Laboratory, University of Notre Dame, Notre Dame, IN 46556, USA

[C] Department of Chemistry and Biochemistry, University of Notre Dame, Notre Dame, IN 46556, USA

[D] School of Electrical and Computer Engineering, Cornell University, Ithaca, NY 14853, USA

[E] Department of Electrical Engineering, University of Notre Dame, Notre Dame, IN 46556, USA

[F] Department of Physics, University of Notre Dame, Notre Dame, IN 46556, USA

[G] Department of Chemical and Biomolecular Engineering, University of Notre Dame, Notre Dame, IN 46556, USA

[H] Department of Materials Science and Engineering, Cornell University, Ithaca, NY 14853, USA

[I] Center for Sustainable Energy at Notre Dame, University of Notre Dame, Notre Dame, IN 46556, USA

[†]These authors contributed equally

[*]Corresponding author, tluo@nd.edu

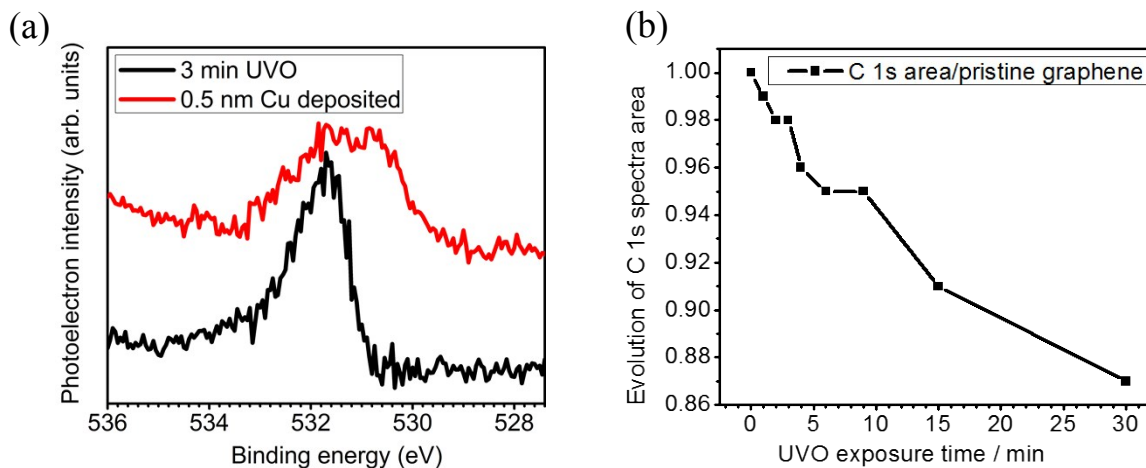**Note 1. XPS and Raman characterizations**

(a)

(b)

Figure S1. (a) XPS characterization of the formation of Cu-O-C covalent bonds between Cu and graphene after Cu is deposited on a 3 min UVO treated graphene. Comparison of O 1s photoemission spectra before and after the Cu deposition. (b) The integrated area of C 1s photoemission spectra for UVO treated graphene versus that area of pristine graphene. The loss of C 1s signal at long exposure time indicates the degradation of graphene.
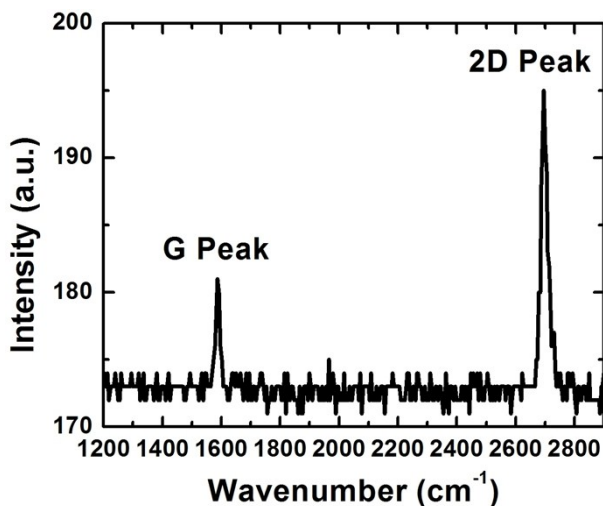
Figure S2. Raman spectrum of graphene synthesized by CVD method. 2D peak shows a much stronger intensity than G peak, indicating the graphene is monolayer.
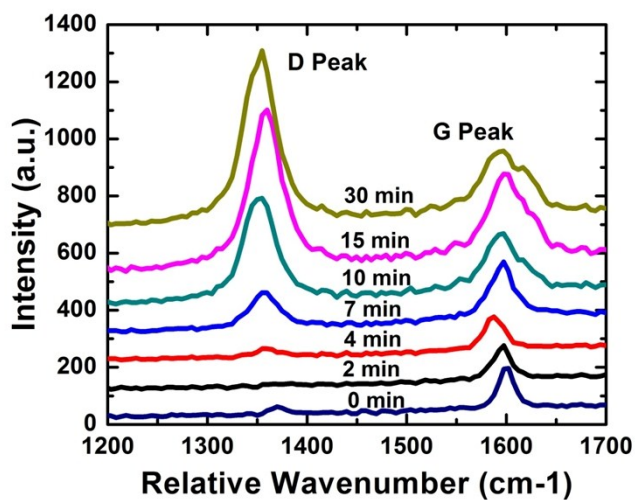
Figure S3. Raman spectra of CVD synthesized monolayer graphene after UVO exposure at various exposure time. At exposure time shorter than 4 min, the absence of D peak on Raman spectra indicates there's little defect on graphene, *i.e.*, graphene is slightly oxidized, while for exposures longer than 4 min, the intensity of D peak rises as the exposure time increases, showing that the longer the UVO exposure time is, the stronger the graphene oxidation becomes. This observation confirms the UVO oxidation effect on graphene, as characterized by XPS in Figure 2 in the main text.

Note 2. TDTR thermal conductance measurements

Note 2.1. Time-domain thermoreflectance (TDTR) Method

The TDTR method[1,2] was employed to measure thermal conductance of the Al/O-Graphene/Cu (O-Graphene is denoted by O-Gr in the following context), Al/Cu/O-Gr/Cu and Al/Pt/O-Gr/Cu interfaces. TDTR method has been widely used to measure the thermal conductivity of materials and interfacial thermal conductance.[2] The TDTR system in our experiment is similar to the one developed by Cahill et al.[2] and Schmidt.[3] It uses a tunable Ti:Sapphire pulsed laser (Spectra Physics, Tsunami) that emits pulses with a duration of ~100 fs and power up to 1.5 W. The laser beam is split into pump and probe beams with central wavelengths at 400 and 800 nm, respectively. The pump beam is modulated by an electro-optic modulator (Conoptics, 350-160) with a sine wave of frequency 5 MHz, while the probe beam passes through a translational mechanical stage (Newport, IMS600PP) to acquire a time delay up to 6 ns. At the sample surface, the pump and probe laser spots have $1/e^2$ diameters of ~60 and ~10 μm, and intensities of ~20 and ~5 mW, respectively. A CCD camera (Edmund Optics, EO-2BW) is integrated in the TDTR for microscopic imaging of the sample, such that high quality regions can be selected for the thermal measurement.

During the TDTR experiment, the Al layer in the substrate is heated by the pump laser and the generated heat transfers to both sides. The probe beam monitors the temperature decay of the Al through the temperature-dependent change in its thermoreflectance at picosecond resolution. After demodulation by a lock-in amplifier (SRS-844), the resultant signal gives amplitude change and phase delay as a function of time. The amplitude or phase signal was fitted by employing heat conduction models to yield the interfacial thermal conductance or thermal conductivity of measured materials.[2]

Note 2.2. Interfacial thermal conductance measurements

Thermal conductance across the interfaces of Al/O-Gr/Cu, Al/Cu/O-Gr/Cu and Al/Pt/O-Gr/Cu was measured using TDTR method. Prior to the measurement, metal Al, Cu and Pt were e-beam evaporated (E-beam evaporator, Oerlikon Univex 450B) on the surface of O-Gr/Cu with thickness of 100, 3 and 10 nm respectively. To take the measurement, the sample was first mounted on the TDTR sample holder with the Al surface facing the incident laser light. The TDTR system was then adjusted to optimize the output signal, and both amplitude and phase signals of the reflected lights were acquired. These signals were fitted using a transient heat conduction model to extract the interfacial thermal conductance. In the fitting, thermal conductivities and specific heats of metal Al and Cu were taken from reference data;[4] the substrate Cu was treated as bulk material while the O-Gr and the layer of Cu (3 nm) or Pt (10 nm) were treated as part of the Al/Cu interface due to their nm-scale thicknesses.[5] Considering the thermal conductivities of Cu and Pt being 400 W/mK and 72 W/mK, respectively, the Cu and Pt layer have conductance values of 133000 and 7200 MW/m^{2}K. The corresponding resistance values are negligible compared to those of the interfaces between metal and graphene. The thermal resistance at the Cu/Al and Pt/Al interfaces should also be negligible since thermal transport at these interfaces is dominated by free electrons, which is usually very efficient.

With all the parameters given, the interfacial thermal conductance is the only unknown quantity in the fitting, thus reliability and accuracy of the results are largely ensured. For each sample, thermal conductance was measured at 6 different locations to obtain the average value. To minimize the experimental noises, 9 sets of data at each measuring location were collected and their average was used for the fitting. Our experimental results show that the thermal measurements are repeatable and consistent for different locations, as exhibited in Figure 3(b).

Note 2.3. Sensitivity analysis of thermal conductance measurement

In TDTR experiments, the signals are collected from the lock-in amplifier (SRS-844). To analyze the sensitivity of data fitting, representative phase signals and their fittings for Al/O-Gr/Cu, Al/Cu/O-Gr/Cu and Al/Pt/O-Gr/Cu interfaces are depicted in Figure S4(a), (c) and (e) respectively, in which the experimental raw data along with curves of best fit, high fit (interfacial conductance G+10%) and low fit (G-10%) are all demonstrated. Also shown in Figure S4 are zoomed views of these phase signals and fittings between 3.0 and 4.5 ns delay time (Figure S4(b), (d) and (f)). As it can be seen, the phase signals show clear trends and agree with the curve hits very well. It is obvious that the best fit and high or low fit are well separated, indicating the thermal conductance values acquired from the best fitting are reliable.
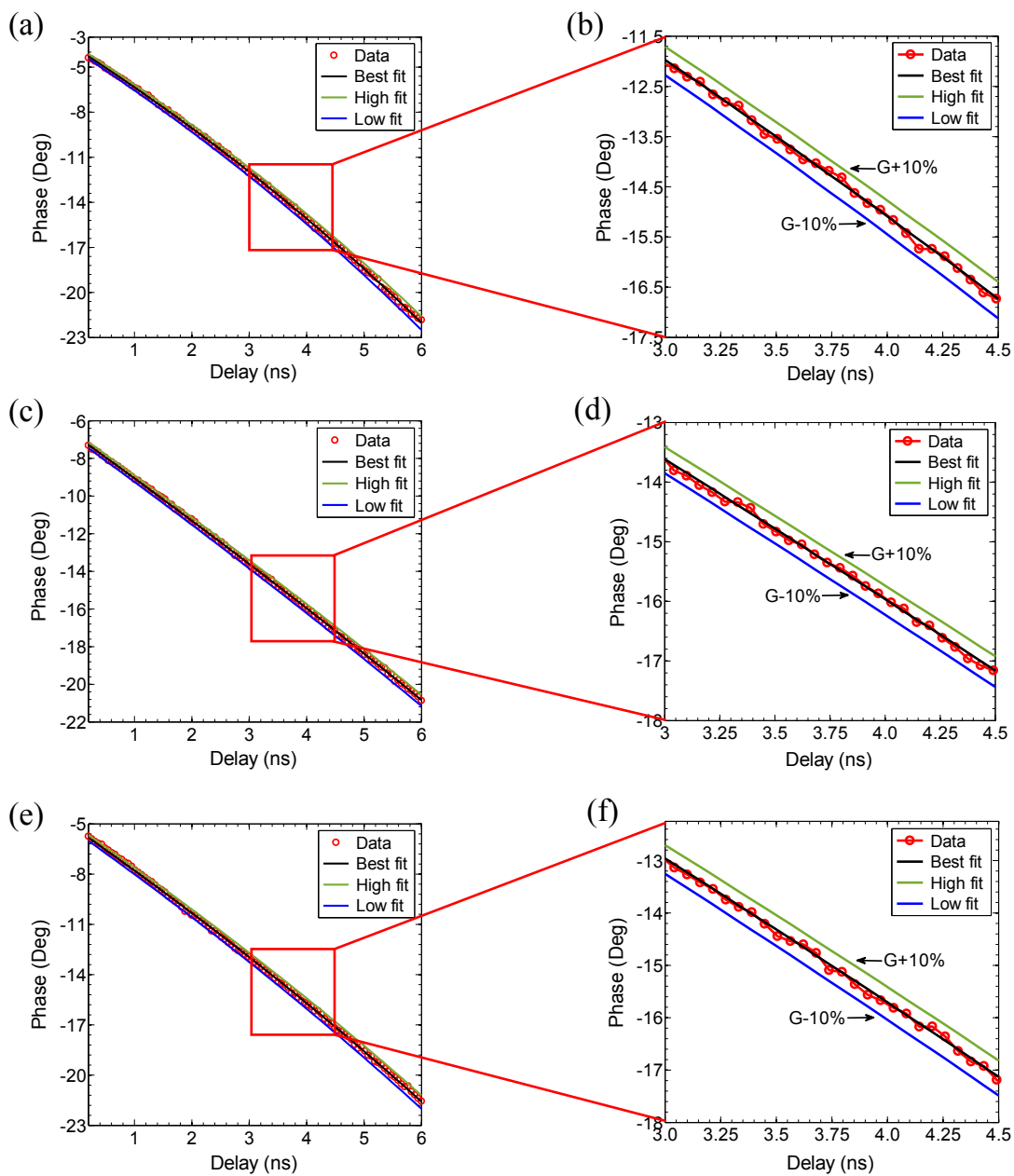
Figure S4. Phase signal along with its best fit, high fit (G+10%) and low fit (G-10%) for the thermal conductance of (a) Al/O-Gr/Cu, (c) Al/Cu/O-Gr/Cu, and (e) Al/Pt/O-Gr/Cu interfaces. In the corresponding close-up views (b) (d) (f), the curves of best fit, high fit and low fit are well separated.

Note 2.4. Uncertainty analyses

In this section we provide analysis of the systematic uncertainty in thermal conductance caused by the uncertainties of the thermal properties (thermal conductivity, specific heat) of metal materials as well as the metal layer thicknesses. The thermal conductivities and specific heats of the involving materials were taken from literatures.[4] The uncertainty of the extracted interfacial thermal conductance can come from the above parameters, which we examine one by one in the following.

Note 2.4.1. Thermal property effect

Simulations of TDTR phase signals at different thermal conductivity K and specific heat C of Al and Cu metals for the Al/Cu/O-Gr/Cu sample are depicted in Figure S5(a) and (b) respectively, in which the black solid line is a simulation using the same K and C values of Al and Cu metals as those in the experiment, whereas the blue circles and red squares designate the simulated phase signals where a 10% uncertainty is introduced to each K and C values for Al and Cu metals, respectively. It can be seen that little changes in the signals are produced by the introduced uncertainties. Moreover, the maximum fluctuation of the extracted thermal conductance, caused by changing Al or Cu thermal conductivity by as much as 10% during the fitting, is obtained as ~4%; and the maximum fluctuation of the extracted thermal conductance, caused by changing Al or Cu specific heat by 10% during the fitting, is ~5%. These fluctuations due to thermal property variations are generally smaller than the deviations of measured thermal conductance at different locations on the sample, which are in the range of 5% – 12% as shown by the error bars in Figure 3(b). Therefore, the uncertainties in the sample thermal properties have small effect on the resultant interfacial thermal conductance.
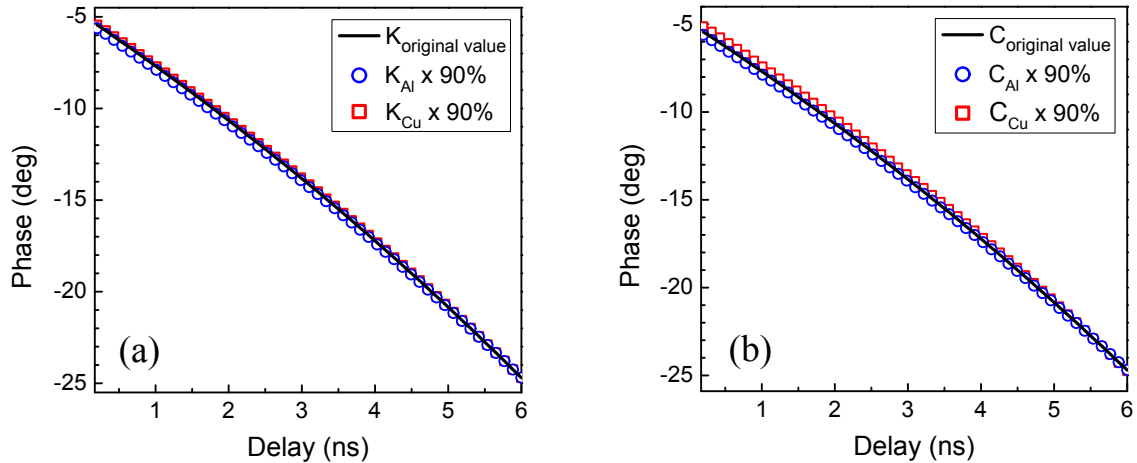
Figure S5. (a) Simulated TDTR phase signals before/after changing the thermal conductivity K of sample components. Black solid line represents the signal using the same thermal conductivities as in the experiment. Blue circles and red squares represent the signals after 10% uncertainties are introduced to Al and Cu thermal conductivities, respectively. (b) Simulated TDTR phase signals before/after changing the specific heat C of sample components. Black solid line represents the signal using the same specific heat values as in the experiment. Blue circles and red squares represent signals after 10% uncertainties are introduced to the Al and Cu specific heats, respectively.

Note 2.4.2. Metal thickness effect

Here we investigate the uncertainty due to the metal film thickness. Experimentally, an Al layer was deposited on the surface of O-Gr/Cu *via* e-beam evaporation (Oerlikon Univex 450B) at a low deposition rate of 1 Å/second to maintain a uniform deposition layer, which also ensures the error of the deposited Al thickness to be far below ±5 nm. We examine the phase signal by changing the Al thickness by ±5 nm. Figure S6 depicts simulations of TDTR phase signals at Al thickness of 100 nm (the experimental value) and 100 ± 5 nm respectively, for the Al/O-Gr/Cu sample (Cu here is treated as a bulk material). The black solid line represents the signal with Al thickness of 100 nm, while the blue circles and red squares represent the signals after changing

9

Al thickness by 100 +/- 5 nm respectively. It is obvious that these three signals are close to each other. The maximum fluctuation of the extracted thermal conductance, caused by changing Al thickness by ±5 nm during the fitting, is obtained as ~7% for Al/O-Gr/Cu sample. It is in the lower range of thermal conductance deviations measured at different locations on the sample, which is 5% – 12% as shown by the error bars in Figure 3(b). Thus, uncertainty in the metal thickness has only a minor effect on our reported values of the thermal conductance.
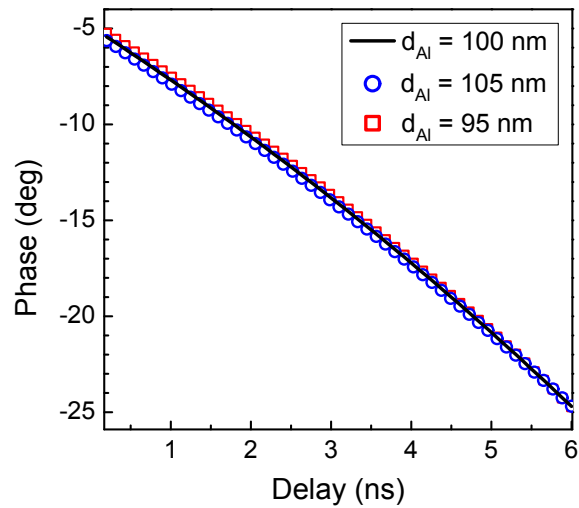

Figure S6. Simulated TDTR phase signals for Al/O-Gr/Cu sample at different Al layer thicknesses. The black solid line represents the signal with Al thickness of 100 nm, same as the experimental value. The blue circles and red squares represent the signals after changing Al thickness by 100 +/- 5 nm respectively.

The above analyses indicate that the systematic uncertainties on thermal conductance caused by uncertainties in the thermal properties and metal layer thicknesses of sample components are relatively small and their influence in the thermal conductance results is indeed minor. It is also worth mentioning that all the samples measured in this work are prepared in one batch, in which each individual sample is almost identical. That is to say, when comparing the interfacial thermal

conductance between samples, quantities like the thermal properties of the metal layers remain the same for all the samples, and as such any uncertainty related to these quantities would have the same influence in all the samples and hence do not affect the resulting trends discussed in the main text. In all, the reliability of the results shown in Figure 3(b) in the main text is ensured.

Note 3. Surface roughness of Cu substrate

Figure S7 shows an atomic force microscopy (AFM) image of a Cu substrate annealed at 1035 °C. The RMS roughness is measured as 2.46 nm over 1 μm × 1 μm area, which is sufficiently smooth for the thermal conductance measurement. We therefore can expect the influence of surface roughness on the measured thermal conductance is limited. Moreover, all the samples are grown on the same copper foil in one batch, and thus even if there is an influence on the thermal conductance data, it will be the same for all the samples. Thus, direct comparison between different samples will not be affected.
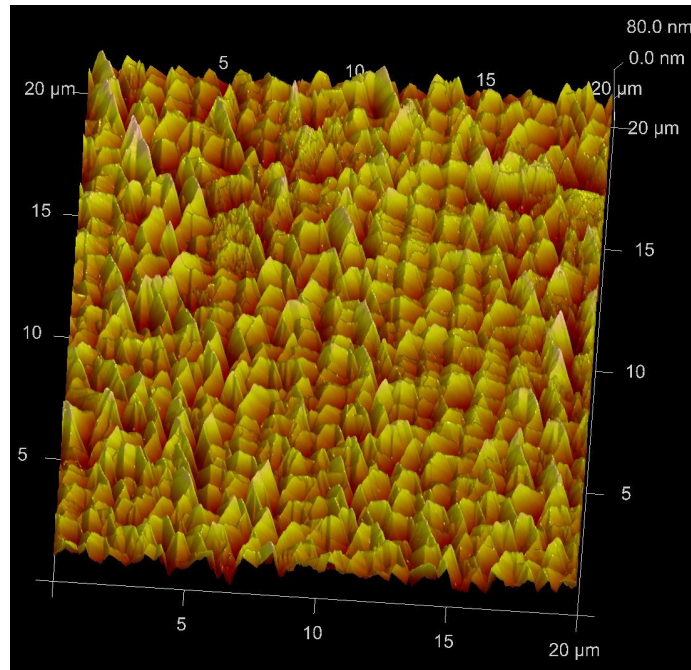
Figure S7. AFM characterization of the surface roughness of a Cu substrate annealed at 1035 °C.

Note 4. Molecular Dynamics (MD) simulation

The large-scale atomic/molecular massively parallel simulator (LAMMPS)[6] is used to perform all the MD simulations in this work. An example structure of Cu/O-Gr/Cu is shown in Figure S8. The Cu substrates have the (100) surfaces exposed to graphene. O atoms are randomly distributed between the Cu substrates and the graphene sheet. We use O coverage defined as the number ratio between O atoms and C atoms to quantify the degree of oxidation of graphene. Periodic boundary conditions (PBC) are used in the x- and the y-directions. PBC is also used in the z-direction for system optimization runs, but isolated boundary condition is used in this direction when calculating thermal conductance. The third generation of charge-optimized many-body (COMB3) potential[7] is used to simulate the interaction between Cu, C and O atoms.
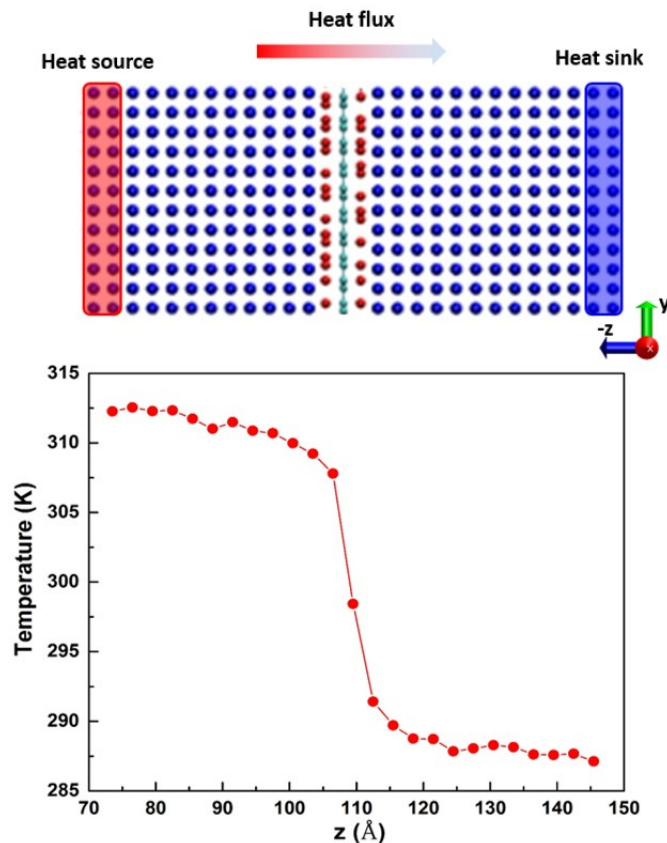
Figure S8. Structure of a Cu/O-Gr/Cu system and an example temperature profile from NEMD simulation. In the structure of a Cu/O-Gr/Cu system, the blue balls represent Cu atoms, the green balls represent C atoms, and the red balls represent O atoms.

The initial structures of the simulated systems are first minimized using the steepest descent algorithm[8]. Then a constant pressure (1 atm) and constant temperature (300 K) ensemble (NPT) is performed on the minimized structure to continue to optimize the structure. The Nose-Hoover method[9,10] is used for the thermostating/barostatting of the NPT ensemble. It is noted again that PBCs in the z-direction are used for the minimization and NPT optimization simulations. Non-equilibrium MD (NEMD) simulations are then performed on the optimized structures to calculate the interfacial thermal conductance.

For NEMD calculations, the end atoms in the z-direction of the system are fixed and isolated boundary condition in this direction is used. In the NEMD simulations, we first run a constant volume and constant temperature (300 K) ensemble (NVT) simulation for 0.1 ns to further equilibrate the system. Then we use a Langevin thermostat[11] to impose a temperature gradient across the simulation domain in the z-direction by setting the temperatures of the two ends at different values, 315 K and 285 K, respectively (Figure S8). A constant volume and constant energy (NVE) ensemble is then used on the system, and the heat flows from the heat source to the heat sink across the sample. When steady state is reached, there is a temperature drop at the Cu/O-Gr/Cu interface in the temperature profile (as shown in Figure S8). During the NVE ensemble run, the energies input into the heat source and removed from the heat sink are recorded and the heat flux (J) is calculated by:

$$J = (dQ/dt)/S \tag{S1}$$

where dQ/dt is the average of the energy input and output rates in the thermostated regions, and S is the cross-sectional area of the system. The interfacial thermal conductance (G) is then calculated by its definition

$$G = J/\Delta T \tag{S2}$$

where ΔT is the temperature drop at the interface. For each simulation, four interfacial thermal conductance values are calculated for four consecutive time blocks in the steady state, and the final interfacial thermal conductance is the average of these four values. The error bar of each interfacial thermal conductance is the standard deviation. All the simulations have the same time step of 0.5 fs. After these NEMD simulations, the overall interfacial thermal conductance of the Cu/O-Gr/Cu system as a function of O coverage was obtained.

Next, for each simulation case, all the O atoms in between the Cu and graphene were deleted, and the NEMD calculation was performed again. This produces the thermal conductance purely due to the vdW contribution since the O atoms are removed and no covalent bonds could form. Because in these simulations the systems are not relaxed, the interface distances stay the same as those before O deletion. Hence, these simulations give thermal conductance as a function of interface distance. We found that the interface distance does not change before and after O deletion. During all these NEMD simulations (including those before and after O deletion), we monitored the average distance between the surface Cu atoms and graphene atoms, and found that the interface distances before and after O deletion are within 2% of each other. Therefore, the vdW interfacial thermal conductance calculated after O deletion is approximately the vdW contribution to the overall interfacial thermal conductance. As a result, the covalent bond contribution can be calculated by subtracting the vdW interfacial thermal conductance from the overall interfacial thermal conductance. Different contributions are shown in Figure 5 in the main text.

References

1. Norris, P. M. *et al*. Femtosecond pump-probe nondestructive examination of materials (invited). *Rev Sci Instrum* 74, 400-406 (2003).
2. Cahill, D. G. Analysis of heat flow in layered structures for time-domain thermoreflectance. *Rev Sci Instrum* 75, 5119-5122 (2004).
3. Schmidt, A. J. in *Optical Characterization of Thermal Transport from the Nanoscale to the Macroscale* Ph.D. Thesis, Department of Mechanical Engineering, MIT (2008).
4. Dillon, C. P. in *CRC Materials Science and Engineering Handbook* Access Intelligence, LLC (2002).
5. Ge, Z., Cahill, D. G. & Braun, P. V. Thermal Conductance of Hydrophilic and Hydrophobic Interfaces. *Phys. Rev. Lett.* 96, 186101 (2006).
6. Plimpton, S. Fast parallel algorithms for short-range molecular dynamics. *J.Comput.Phys.* 117,

1-19 (1995).

7. Liang, T. *et al*. Classical atomistic simulations of surfaces and heterogeneous interfaces with the charge-optimized many body (COMB) potentials. *Mat. Sci. Eng: R: Rep.* 74, 255-279 (2013).

8. Arfken, G. in *Mathematical methods for physicists* 428-436 Orlando, FL: Academic Press (1985).

9. Nose, S. A unified formulation of the constant temperature molecular dynamics methods. *J.Chem.Phys.* 81, 511-519 (1984).

10. Hoover, W. G. Canonical dynamics: Equilibrium phase-space distributions. *Phys. Rev. A* 31, 1695-1697 (1985).

11. Schneider, T. & Stoll, E. Molecular-dynamics study of a three-dimensional one-component model for distortive phase transitions. *Phys. Rev. B* 17, 1302-1322 (1978).